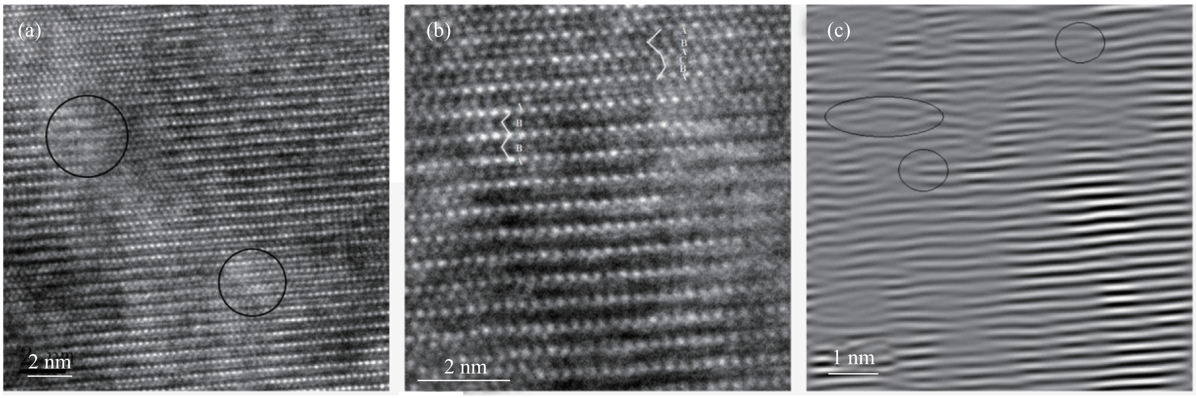

Fig. 4 (a) High-resolution XTEM micrographs image of GaN with He-ion implantation to fluence of 2×10^{16} cm^{-2}. (b) High-magnification image showing that the stacking faults in the damaged layer. (c) Fourier-filtered (0002) diffraction high-magnification image.

References

[1] B. S. Li, Z. G. Wang, J. Phys. D: Appl. Phys, 48(2015)22510.

[2] J. F. Barbot, F. Pailloux, M. L. David, et al., J. Appl. Phys., 104(2008)043526.

[3] C. M. Wang, W. Jiang, W. J. Weber, et al., J. Mater. Res., 17(2002)2945.

4 - 2 H-ion Irradiation-induced Annealing in He-ion Implanted 4H-SiC

Han Yi[1,2] , Li Bingsheng[1] and Wang Zhiguang[1]

([1]Institute of Modern Physics, Chinese Academy of Sciences, Lanzhou 730000, China;
[2]University of Chinese Academy of Sciences, Beijing 100049, China)

Silicon carbide and silicon carbide matrix composites are widely applied in various fields because of their excellent performance. SiC materials have a lot of advantages such as high melting point, high corrosion resistance, high heat conductivity and low neutron reaction cross section, *etc.* Therefore, SiC materials is very suitable for advanced nuclear power plant (fusion reactor and fission reactor), accelerator driven sub-critical nuclear power system with high temperature and high flux neutron irradiation environments. Neutron irradiation can cause serious displacement damage in the material, and helium atoms caused by neutron transmulation reaction agglomate into the material to form helium bubbles, which can cause swelling and helium embrittlement. As a result, the performance of materials is serious deteriorated. At the same time, the proton produced by nuclear reaction can also cause displacement damage in the material. Up to now, the effects of irradiation with a single kind of ion into SiC have been extensively researched, while the effects of dual beam or more beam irradiation into SiC were less researched.

Part of single crystal 4H-SiC wafers were implanted with 230 keV He^+ ion at room temperature (RT) with fluences in the range $1.0\times10^{15} \sim 2.0\times10^{16}$ ions/cm^{-2} (0.04 ∼0.8 dpa). Then some 4H-SiC wafers were irradiated with 260 keV H^+ ion at room temperature with fluence of 5.0×10^{15} ions/cm^{-2} (0.2 dpa). Raman spectroscopy was performed to investigate the behavior of single crystal 4H-SiC under irradiation. The program SRIM-2008 simulates the lattice damage peak of He ion implanted 4H-SiC by using the molecular dynamics (MD) simulations, as shown in Fig. 1. Through the program SRIM-2008 simulation we can get that He ion implanted 4H-SiC lattice damage peak is at 750 nm from the surface.

Fig. 2(a) shows the Raman spectra of 4H-SiC before and after implantation with He ions to fluences of 1.0×10^{15}, 5.0×10^{15}, 8.0×10^{15}, 1.0×10^{16} and 2.0×10^{16} cm^{-2}. It should be noted that the characteristic peaks of the samples after He implantation do not undergo lateral shift, which indicates that the He implantation-induced stress is not enough to cause the offset of Raman peaks. The Raman spectra of 1.0×10^{15} cm^{-2} ion implanted sample have no significant change compared with that of the as-grown sample. With increasing the fluence, the width of A_1(LO) peak decreases obviously. Because phonon lifetime is inversely proportional to the peak width, He implantation reduces carrier concentration profiles, resulting in decreasing the scattering probability and increasing the phonon lifetime. When fluence increases to 8.0×10^{15} cm^{-2}, there are three new Raman scattering peaks at 200, 540 and

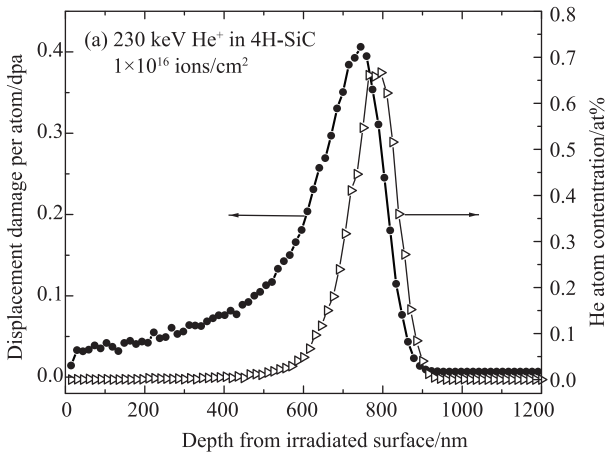

Fig. 1 Example of depth distribution of rates of displacement damage and concentration of He in 4H-SiC calculated by SRIM-2008. The displacement threshold energy was 20 and 35 keV for C and Si atom, respectively.

660 cm^{-1}, corresponding to crystalline Si(TA), crystalline Si(TO) and disordered SiC Raman spectra, respectively. It is well known that pre-existing chemical bonds break to form new Si–Si and C–C bonds in the disordered SiC. In addition, the E_2(TA), A_1(LA), and E_1 (TO) characteristic peaks of Raman spectra completely disappear. The intensities of Raman spectra decrease due to the increase of the absorption of Raman scattering.

It is a usual method to calculate the SiC total disorder based on the Raman peaks relative strength. In this work, the area of E2(TO) Raman peak is used to calculate the relative disorder intensity. Fig. 2(b) shows that the disorder of the sample increases with the fluence. The damage accumulation versus implantation fluence can be divided into two stages (0~0.24 dpa and 0.24~0.8 dpa). In the first stage (0~0.24 dpa), the irradiation area mainly consists of point defects and small clusters, corresponding to the low damage level. At the second stage (0.24~0.8 dpa), the damage level rapidly increases with the fluence. The relative Raman intensity equals to 1 at 0.32 dpa, corresponding to the dimorphous phase formed in the damage layer.

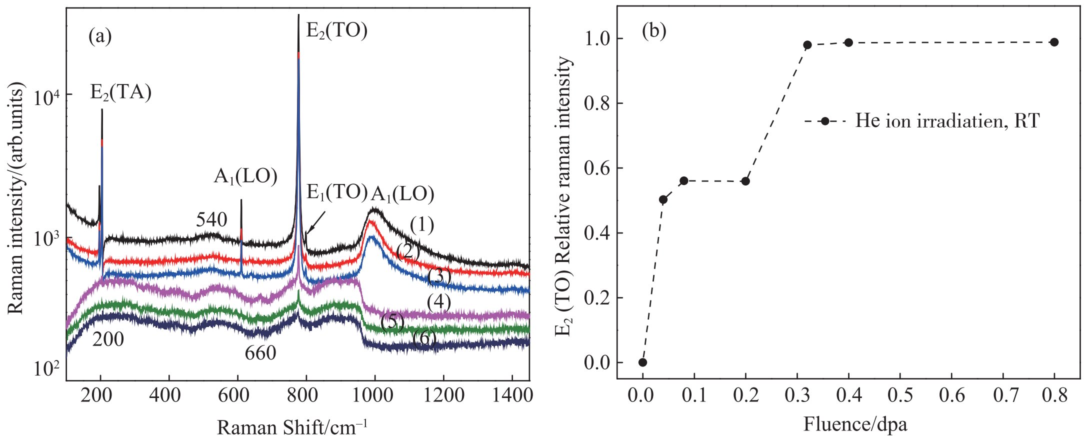

Fig. 2 (color online) Raman spectra of He-implanted 4H-SiC to fluences of 1.0×10^{15} cm^{-2} (2) 5.0×10^{15} cm^{-2} (3) 8.0×10^{15} cm^{-2} (4) 1.0×10^{16} cm^{-2} (5) and 2.0×10^{16} cm^{-2} (6) at room temperature, compared with the as-grown sample (1). (b) The relative Raman intensity of He-implanted 4H-SiC at room temperature is plotted versus the fluence of E_2 (TO).

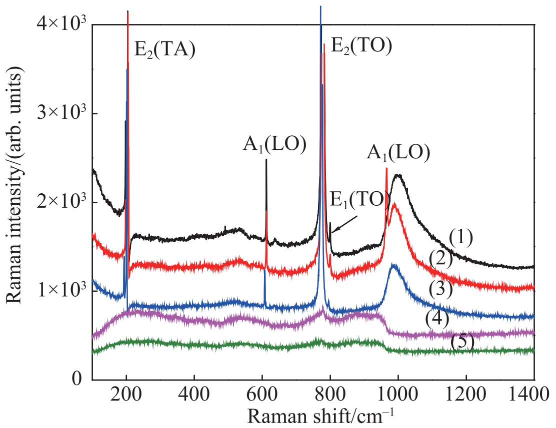

Fig. 3 (color online) Raman spectra of He-implanted 4H-SiC to fluences of 5.0×10^{15} cm^{-2} (3) and 2.0×10^{16} cm^{-2} (5) at room temperature, post-He implantation, H irradiation to a fluence of 5.0×10^{15} cm^{-2} at room temperature for the low fluence He-implanted sample (2) and the high fluence He implanted sample (4), compared with the as-grown sample (1).

Fig. 3 shows that the intensities of the E_2(TA), A_1(LO), E_2(TO), E_1(TO) and A_1(LO) peaks increase after H irradiation, indicating pre-existing defect recovery after H irradiation. The Raman intensity increment is related to the pre-existing damage level. In detail, the Raman intensity increment is more significant at a lower initial damage level, as shown in Fig. 3. Other data proves the damage recovery, that a strong new peak appears nearly at 966 cm^{-1}, which is assigned to 3C-SiC LO (Γ) presented in Fig.3. It is well known that the 3C-SiC structure nucleates in amorphous layers of hexagonal SiC by thermal annealing and by ion-beam induced epitaxial recrystallization. The present experimental results demonstrate that H irradiation plays a role the same as thermal annealing. The pre-existing defect recovery upon H irradiation is suggested to originate from ion beam induced epitaxial crystallization. However, the necessary ion fluence of 1.0×10^{17} cm^{-2} is too high for practical application. In the present work, we use 260 keV H^+ ion irradiation to a fluence of 5.0×10^{15} cm^{-2} at room temperature. Though almost no effects of H irradiation on an amorphous layer are formed in He-implanted 6H-SiC, the significant recrystallization of He-implanted 4H-SiC with a relative damage of 0.55 occurs after H irradiation. This is very useful for practical applications. For example, in the nuclear radiation environments, dense energetic H and He atoms are produced simultaneously. Therefore, the He implantation-induced defects can be annealed out upon H irradiation immediately, indicating that the amorphous phase has never been formed under such a condition. The present experimental results demonstrate a strong reduction of the damage production to extend SiC material lifetime in nuclear reactors.

References

[1] V. Heera, J. Stoemenso, R. Koler, et al., J. Appl. Phys., 77(1995)2999.

[2] Y. W. Zhang, R. Sachan, O. H. Pakarinen, et al., Nat. Commun., 6(2015)8049.

4 - 3 An Experimental Setup for High Temperature and High Pressure Fluid Flow Effects

Ma Zhiwei, Wang Zhiguang, Liu Chao, Sun Jianrong, Chang Hailong, Li Bingsheng,
Sheng Yanbin and Pang Lilong

In order to accumulate the experimental data for building accelerator driven sub-critical systems (ADS), a high temperature and high pressure water circuit setup has been built. It is mainly used to study heat transfer deterioration of high temperature and high pressure water vapor in the circuit, flow instability mechanism and heat exchange efficiency of fuel rod in primary loop. Lots of similar experimental setups have been built by scientific research institution around the world[1−3]. Unlike the existing experimental setup, flow rate of high temperature and high pressure water vapor was considered as a significant parameter to study above-mentioned research proposal.

The operating temperature of the experimental setup was designed to be 300 ℃∼650 ℃ and the operating pressure is 8∼10 MPa. The main parameters of the experimental setup are shown in Table 1.

Table 1 The relevant parameters of the experimental setup.

Parameters	Values
Operating temperature/ ℃	300∼650
Operating pressure/ MPa	0.1∼10
Flow rate/(m/s)	0∼10
The conductivity of deionized water/ (μs/cm)	≤ 0.1
The dissolved oxygen content of deionized water/ppb	≤ 10
Inlet temperature/ ℃	300
Length of test section/mm	1 500

The flow chart of setup shown in Fig. 1 and the side view of setup shown in Fig. 2.

The experimental setup consists of three components:

1) Deionized water preparation and deoxidization system: Deionized water was prepared by deionized water preparation machine and the conductivity of water can be less than 0.1 μs/cm. Then deionized water was deoxygenized by injecting nitrogen to make the oxygen content below 10 ppb and the dissolved oxygen content can be controlled by nitrogen feedback regulation.

2) Heating and experimental system: Deionized water was pumped into circulation loop by a high-pressure plunger pump. The water was preheated up to 300 ℃ by electro-magnetic induction furnace and then heated by heating pipe in chamber. Thermometer probes and piezometers were set in the loop to collect data.

3) Experimental control and data collection system: The experimental setup was controlled by a control cabinet and software on computer. Experimental data can be real-time acquired by software.

Some tests have been done when flow rate was set as 5 m/s and 8 m/s. It turned out that the experimental setup can run stably. The mid-section steam temperature can reach up to 360 ℃ and remained stably when flow rate was 5 m/s (Fig. 3(a)). The medium-frequency heating power was 7.5 kW at the beginning and then decreased to 2.0 kW after heating for 70 min (Fig. 3(b)). The mid-section steam temperature can reach up to 350 ℃ when flow rate was 8 m/s(Fig. 4(a)). The medium-frequency heating power was 22 kW and maintain steady basically (Fig. 4(b)).